Time-dependent calculations of double photoionization of the aligned H_2 molecule

I. A. Ivanov* and A. S. Kheifets†

Research School of Physical Sciences, The Australian National University, Canberra ACT 0200, Australia

(Received 31 October 2011; published 10 January 2012)

We perform time-dependent calculations of single-photon two-electron ionization of the aligned H_2 molecule by an xuv pulse. Solution of the time-dependent Schrödinger equation is sought in spherical coordinates on a radial grid by time propagation using the Arnoldi-Lanczos method. From these calculations, we derive the total integrated as well as fully differential ionization cross sections for equal energy sharing and various orientations of the internuclear axis relative to the polarization vector of light. Satisfactory agreement with available literature data validates the present theoretical model. We supplement our numerical computations with an amplitude analysis of differential cross sections using the atomiclike formalism of Feagin [J. Phys. B **31**, L729 (1998)]. This analysis provides some additional insight into mechanisms of double photoionization of the aligned H_2 molecule.

DOI: 10.1103/PhysRevA.85.013406 PACS number(s): 32.80.Rm, 32.80.Fb, 42.50.Hz

I. INTRODUCTION

The single-photon two-electron ionization (double photoionization or DPI) of the H_2 molecule became a subject of renewed interest after experimental data resolved with respect to the molecular-axis orientation became available [1–3]. In these kinematically complete, four-body fragmentation experiments, a strong dependence of the photoelectron angular distribution on the orientation of the molecular axis was demonstrated. This observation was not possible in earlier measurements on randomly oriented H_2 or D_2 molecules [4–7], which could be described rather adequately by atomiclike analytical models [8,9] or central-field numerical computations [10,11]. The new set of molecular-orientation-specific DPI measurements gave an impetus to the rapid advancement of theory. First, *ab initio* nonperturbative calculations of the total integrated cross section (TICS) were reported using the time-dependent close-coupling (TDCC) [12] and the exterior complex scaling (ECS) [13] methods. These integrated cross-section data were found in a much better agreement with experiment [14,15] than the earlier perturbative calculations [16,17]. Next, triply differential cross sections (TDCS) resolved with photoelectron momenta and specific to molecular orientation were evaluated within the ECS [18] and TDCC [19] methods. The two sets of TDCS calculations were found in good agreement with each other and, after convolution with the instrumental function, fit the experimental data rather well. These initial reports were followed by two subsequent calculations performed in prolate spheroidal coordinates using grid-based [20] and time-dependent [21] methods. The TDCC data were also reevaluated by using a bigger box size and achieving better convergence [22]. A detailed comparison of the latest TDCS results [21] showed some model dependence, which could not be unambiguously resolved by experiment because of its uncertainties in the molecular alignment and the emission angles of the photoelectrons. Nevertheless, the two calculations [21,22] were found particularly close and could serve as a practical benchmark for further development of theory.

Apart from various numerical models, valuable insight into molecular DPI can be gained from qualitative analysis based on quantizing rotations of the momentum plane of the electron pair about its relative momentum [8]. In this analysis, the molecular DPI in the laboratory frame is represented by a pair of amplitudes, g_Σ and g_Π. These amplitudes are defined in the molecular frame and correspond to the parallel $\boldsymbol{e} \| \hat{\boldsymbol{R}}_N$ and perpendicular $\boldsymbol{e} \perp \hat{\boldsymbol{R}}_N$ orientations of the internuclear axis and polarization vector of light, respectively. This technique was very efficient in its description of the DPI of randomly oriented H_2 molecules [4–6]. It was successfully extended to account for recent observations of noncoplanar electron-pair, molecular-axis angular distributions [28], where the molecular-orientation effects were particularly stark. To account for these effects, the atomiclike $S \to P$ transition in the electron-pair total angular momentum should be supplemented by the $S \to D$ and $S \to F$ contributions which are specific to molecular DPI.

This state of numerical modeling and analytical analysis of the DPI process in H_2 gives a starting point to the present work, which has a dual purpose. First, we want to extend our time-dependent calculations of the strong-field ionization of atoms (hydrogen [23], helium [24], and lithium [25]) to molecular targets. Our approach is based on the numerical solution of the time-dependent Schrödinger equation (TDSE) in spherical coordinates on a radial grid by time propagation using the Arnoldi-Lanczos method. By projecting this solution onto the field-free states of the molecular H_2^+ ion, we obtain probabilities and cross sections for various ionization channels. This approach is similar to that taken in Ref. [21], except that instead of prolate spheroidal coordinates, we employ spherical coordinates. We test our calculations of the TICS of the DPI of H_2 across a wide range of photon energies against the most recent and consistent sets of experimental and theoretical data [12,13,15]. We also perform TDCS calculations for equal energy sharing at two fixed photon energies. The first photon energy of 75 eV is chosen to test the accuracy of the present model by making a comparison with the benchmark data [21,22]. Coincidentally, this photon energy falls close to the center of a broad Cooper-like minimum in the dipole channel of the single photoionization of H_2 for the parallel-field orientation [26]. The second photon energy of

*igor.ivanov@anu.edu.au
†a.kheifets@anu.edu.au

120 eV is selected well outside this minimum. By comparing TDCS at these two selected photon energies, we evaluate the influence of the Cooper minimum in the single-ionization channel on the DPI process.

Our second goal is to study the underlying many-body dynamics behind the molecular DPI process. This is achieved by analyzing the TDCS of the DPI on the aligned H_2 molecule in terms of the amplitudes g_Σ and g_Π given in the atomiclike formalism of Feagin [8]. We perform this analysis using the parallel $\boldsymbol{e} \| \hat{\boldsymbol{R}}_N$ and perpendicular $\boldsymbol{e} \perp \hat{\boldsymbol{R}}_N$ coplanar TDCS at the equal energy sharing. We find that the case of perpendicular-field orientation is described rather well by a single amplitude g_Π for all mutual orientations of the reference photoelectron relative to the internuclear axis. This amplitude is well fitted by the Gaussian ansatz and is rather similar to the symmetric amplitude of the DPI of He at the corresponding excess energy. The coplanar TDCS in the case of parallel-field orientation can also be described by the corresponding amplitude g_Σ. However, this amplitude demonstrates some variation with the reference photoelectron fixed angle. Most strikingly, this amplitude shows a very strong deviation from the Gaussian ansatz and can only be fitted by a di-Gaussian parametrization. This distortion of the amplitude is typical for the DPI of various L-shell atomic targets whose radial orbital has a node [27].

It is well documented that the dipole approximation fails most strongly for the noncoplanar DPI of H_2 [3,28]. This failure can be attributed to a strong Cooper-like minimum in the dipole channel of the single photoionization of H_2 for the Σ orientation at the photon energy close to 75 eV [26]. It may also be for the same reason that the Gaussian ansatz fails for the coplanar TDCS in the parallel-field orientation. To test this hypothesis, we repeated our TDCS calculations at a much higher photon energy of 120 eV, well away from the Cooper minimum in the dipole channel. Much to our surprise, the same pattern of the coplanar TDCS was observed. The TDCS for perpendicular-field orientation was very well fitted by the Gaussian ansatz to the amplitude g_Π, but an analogous fit for the parallel-field orientation required the strongly non-Gaussian amplitude g_Σ.

The paper is organized as follows. In Sec. II, we give details of our computational method implementing the numerical solution of the TDSE (Sec. II A) and extraction of various DPI cross sections (Sec. II B). In Sec. III, we present our numerical results for the total (Sec. III A) and triply differential (Sec. III B) cross sections. We conclude in Sec. IV by proposing possible extensions of the present work.

II. COMPUTATIONAL DETAILS

A. Solution of the TDSE

We consider the evolution of the H_2 molecule in the presence of an xuv pulse,

$$\boldsymbol{E}(t) = \boldsymbol{E}_0 f(t) \cos \omega t, \tag{1}$$

with the carrier frequency $\omega = 75.5$ eV and the peak field strength $E_0 = 0.1$ a.u. (corresponding to the intensity of 3.5×10^{14} W/cm^2). The pulse is switched off outside the time interval $(0,10T)$, where $T = 2\pi/\omega$ is an optical cycle of the carrier frequency. The envelope function $f(t)$ is chosen in such a way that the amplitude of the xuv field is ramped on and off smoothly during one optical cycle T, and is constant in between. In the following, we consider cases of parallel and perpendicular mutual orientations of the xuv field and the H_2 molecule, which is assumed to be oriented along the quantization axis $\hat{\boldsymbol{R}}_N \| z$. The field is linearly polarized along the z or x axes for parallel or perpendicular orientations, respectively.

We solve numerically the TDSE for the H_2 molecule interacting with the xuv field,

$$i\, \partial\Psi/\partial t = [\hat{H}_{\rm mol} + \hat{H}_{\rm int}(t)]\Psi, \tag{2}$$

where $\hat{H}_{\rm mol}$ is the Hamiltonian of a field-free hydrogen molecule and the operator $\hat{H}_{\rm int}(t)$ describes molecule-field interaction. We choose the velocity form for this operator,

$$\hat{H}_{\rm int}(t) = \boldsymbol{A}(t) \cdot (\hat{\boldsymbol{p}}_1 + \hat{\boldsymbol{p}}_2), \tag{3}$$

with the vector potential $\boldsymbol{A}(t) = -\int_0^t \boldsymbol{E}(\tau) d\tau$.

The Hamiltonian operator is discretized on a spatial grid $\{r_i\}$ composed of several intervals with a progressively increasing step size. The wave function at the grid points is represented as a partial wave expansion,

$$\Psi(\boldsymbol{r}_1,\boldsymbol{r}_2) = \sum_{l_1,l_2,J} f^J_{l_1 l_2}(r_1,r_2) |l_1(1) l_2(2)\; J\rangle. \tag{4}$$

Here the notation $|l_1(1)l_2(2)\; J\rangle$ is used for bipolar harmonics [29], and summation is restricted to $l_1, l_2 = 0-6$ with the total angular momenta $J = 0-5$.

The initial $^1\Sigma_g$ state was prepared by using imaginary-time propagation of the field-free H_2 molecule (relaxation procedure) starting from some trial wave function. Using this procedure, we obtained the ground-state energy of -1.167 a.u. at the equilibrium internuclear distance $R = 1.401$ a.u. This value corresponds to the Coulomb interaction of nuclei included in the Hamiltonian, i.e., it represents the total energy of the hydrogen molecule. More useful characteristics of the initial state in our problem, where the nuclei are kept fixed and their repulsion energy in the initial and final states cancels out, is the value obtained if the term $1/R$ is subtracted from the Hamiltonian. This subtraction gives us the value of -1.8807 a.u. for the double-ionization potential, in good agreement with the literature data.

With this initial state, the solution of the TDSE was propagated in time over the interval $(0,20T)$ using the Arnoldi-Lanczos method [30,31]. After the field pulse is off for $t > 10T$, the system evolves freely. Information obtained using this field-free evolution after the end of the pulse can be used to assess the accuracy of the TDSE solution.

B. Final states and extraction of DPI cross sections

To extract various DPI cross sections from the solution of the TDSE, we project this solution after the end of the pulse on the set of the doubly ionized states of the H_2 molecule, $\Psi^-_{\boldsymbol{k}_1,\boldsymbol{k}_2}(\boldsymbol{r}_1,\boldsymbol{r}_2)$, with ingoing boundary conditions. These states are constructed from ingoing scattering states of the H_2^+ molecular ion with asymptotic momenta $\boldsymbol{k}_1$ and $\boldsymbol{k}_2$. The latter are found as follows.

First, we prepare a one-electron basis set $\Psi_{k\,l_0M}(\boldsymbol{r})$ of the continuum spectrum of the H_2^+ ion. These states are obtained as eigenfunctions of the H_2^+ Hamiltonian corresponding to a given value of the angular momentum projection M on the internuclear axis $\hat{\boldsymbol{R}}_N$, and a given positive energy $E = k^2/2$. We represent these states as

$$\Psi_{k\,l_0M}(\boldsymbol{r}) = \sum_{l \geqslant |M|} r^l g_{k\,ll_0M}(r) Y_{lM}(\hat{\boldsymbol{r}}), \tag{5}$$

with the boundary conditions at the origin $g_{k\,ll_0M}(0) = \delta_{ll_0}$. The substitution of this expansion in the Schrödinger equation for the positive-energy eigenstates of the H_2^+ ion gives a set of equations for the functions $g_{k\,ll_0M}(r)$. Now we can represent the ingoing scattering states of the H_2^+ ion as

$$\Psi^-_{\boldsymbol{k}}(\boldsymbol{r}) = \sum_{l_0M} a_{l_0M} \Psi_{k\,l_0M}(\boldsymbol{r}). \tag{6}$$

The coefficients a_{l_0M} can now be found from the requirement that in each partial wave, the terms containing outgoing exponentials e^{ikr} coincide for $r \to \infty$ with those of the ingoing scattering state for the hydrogenlike ion with the nuclear charge $Z = 2$.

The differential probability of the DPI can now be found as

$$P(\boldsymbol{k}_1, \boldsymbol{k}_2) = \left| \left\langle \Psi^-_{\boldsymbol{k}_1,\boldsymbol{k}_2} \middle| \Psi(t) \right\rangle \right|^2, \tag{7}$$

where $\Psi(t)$ is the solution of the TDSE at the moment of time after the end of the xuv pulse. When computing this overlap, we use the recipe proposed in Ref. [32] to remove unwanted contributions of the bound and singly ionized states. This procedure suggests that all of the radial integrals entering the overlap (7) should be computed starting from some value $r = R_0$ or, equivalently, $\Psi(t)$ should be set to zero if either $r_1 < R_0$ or $r_2 < R_0$. The rationale behind this recipe is the following. If we wait long enough, the wave packet describing the doubly ionized states leaves the region where either $r_1 < R_0$ or $r_2 < R_0$. Outside this region, the part of the wave function describing the contributions of bound and singly ionized states is heavily dumped due to the bound character of at least one of the electrons. We can expect that if we choose R_0 and the moment of time t after the end of the pulse appropriately, then we can avoid contamination of the DPI process by singly ionized or bound channels.

The differential probability (7) is converted into the cross section in a usual way. First, we should take into account the fact that the TDCS is defined on the energy shell which corresponds to the strict energy conservation. For the pulse of a finite duration (1), the energy is conserved only approximately. Therefore, we have to employ a procedure [21,33] which corrects for this fact, effectively reducing differential probabilities to energy shell only. For the case of equal energy sharing between the two photoelectrons, the corresponding formula reads

$$P^{\rm av}(E_1, \hat{\boldsymbol{k}}_1, \hat{\boldsymbol{k}}_2) = \frac{1}{E_1} \int_0^\infty P(u\hat{\boldsymbol{k}}_1, u\hat{\boldsymbol{k}}_2) u\,du, \tag{8}$$

where $E_1 = E_2$ is the energy of an escaping electron. Physically, this procedure corresponds to averaging the differential probability over the whole region of electron momenta, keeping the ratio of electron energies constant. Finally, we have to convert the averaged probability $P^{\rm av}$ into the differential cross section as

$$\frac{d^3\sigma}{dE\,d\hat{\boldsymbol{k}}_1\,d\hat{\boldsymbol{k}}_2} = \frac{8\pi\omega}{c} \frac{P^{\rm av}(E, \hat{\boldsymbol{k}}_1, \hat{\boldsymbol{k}}_2)}{W}, \tag{9}$$

where $W = 2\int_0^{10T} E^2(t)dt$ and $c \approx 137$ is the speed of light in atomic units.

III. NUMERICAL RESULTS

A. Total integrated cross sections

The total integrated cross section (TICS) of the DPI of H_2as a function of the photon energy is shown on the left panel of Fig. 1. The present TDSE results are compared with the TDCC [12] and the ECS [13] calculations as well as the experiment [15]. The ECS result is shown in the velocity gauge. The corresponding length gauge result is only marginally different. The theoretical data are the sum of cross sections for parallel and perpendicular orientations of the internuclear axis relative to the field. The experimental data are taken at random orientation of the internuclear axis.

Some information on the molecular-orientation dependence of the TICS can be gained from the right panel of Fig. 1, where we compare the cross-section ratios for perpendicular- versus parallel-field orientations. The DPI ratio $\sigma_\Pi^{2+}/\sigma_\Sigma^{2+}$ from the ECS calculation [13] is shown by a thin black line, whereas the single-photoionization ratio $\sigma_\Pi^{+}/\sigma_\Sigma^{+}$ from the RPA calculation [26] is displayed with a thick blue line. The single-photoionization ratio peaks at the photon energy of about 75 eV, which corresponds to a Cooper-like minimum in the dipole channel for the parallel-field orientation. This maximum is replicated in the DPI cross-section ratio at a slightly lower photon energy. Generally, the Π-to-Σ ratios are similar in the single- and double-photoionization channels. This allows one to speculate that the two-step mechanism of the DPI of H_2 is dominant in this photon-energy range. In other words, DPI proceeds via the single photoionization of H_2 and subsequent electron-impact ionization of the H_2^+ ion. This second stage of the DPI process is also dependent on

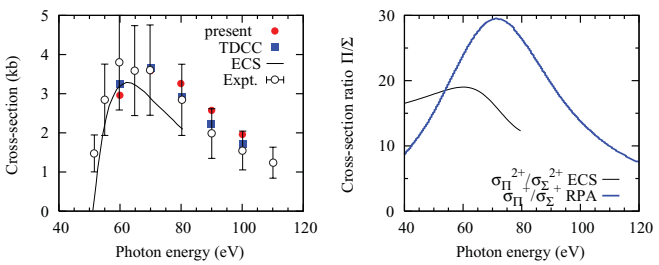

FIG. 1. (Color online) Left panel: Total integrated cross section of the DPI of randomly oriented H_2 as a function of photon energy. Present TDSE results (red filled circles) are plotted along with the TDCC calculation (blue filled squares) [12], the ECS calculation (black solid line) [13], and the experiment [15]. Right panel: Cross-section ratios for perpendicular- and parallel-field orientations. The DPI ratio $\sigma_\Pi^{2+}/\sigma_\Sigma^{2+}$ from the ECS calculation [13] is shown by a thin black line, whereas the single-photoionization ratio $\sigma_\Pi^{+}/\sigma_\Sigma^{+}$ from the RPA calculation [26] is displayed with a thick blue line.

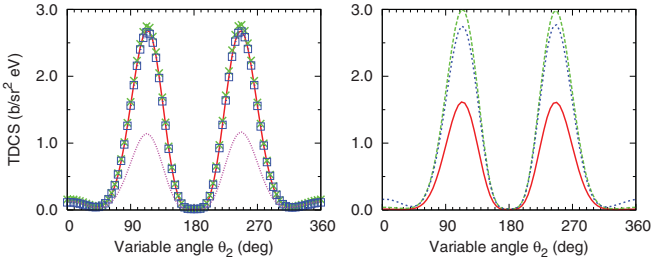

FIG. 2. (Color online) Coplanar TDCS of the DPI of H_2 at photon energy of 75 eV and equal energy sharing. The angle of the internuclear axis, $\theta_N = 90^\circ$, and the fixed reference photoelectron angle, $\theta_1 = 0^\circ$. Left panel: Results obtained for $t = 16T$, and $R_0 = 5$ (red solid line), 10 (green crosses), 15 (blue boxes), and 25 a.u. (magenta dots). Right panel: Results obtained for $R_0 = 10$ a.u., and $t = 10T$ (red solid line), $14T$ (green dashed line), and $16T$ (blue dots).

the molecular orientation, but its angular anisotropy is much weaker than that of the single photoionization.

B. Differential cross sections

1. Stability test

Before presenting a complete set of TDCS calculations, we show some results of the stability test. Our numerical procedure is based on the expectation that there exists a range of distances R_0 and the time interval t where projection of the solution of the TDSE on the field-free molecular states produces stable results. As illustrated in Fig. 2, these expectations are well founded. In this figure, we present a coplanar TDCS of the DPI of H_2 at the photon energy of 75 eV and equal excess energy sharing between the two photoelectrons. The angle of the internuclear axis, $\theta_N = 90^\circ$, and the fixed reference photoelectron angle, $\theta_1 = 0^\circ$, are both measured relative to the polarization vector of light. One can see from the figure that varying parameter R_0 between 5 and 15 a.u. produces virtually no effect on the TDCS. For larger values of R_0, results start changing quickly. By using $R_0 = 25$ a.u. and $t = 16T$, we simply do not give the doubly ionized wave packet enough time to leave the region where either $r_1 < R_0$ or $r_2 < R_0$. As shown in Fig. 2, computing the projection at $t = 16T$ gives us a comfortably large interval of R_0 to implement the recipe of Ref. [32] . All results presented below have been obtained for $R_0 = 10$ a.u.

Similarly, the right panel of Fig. 2 shows that if we let the system evolve sufficiently far in time using the fixed value of R_0 for the cutting parameter of the projection operation, we obtain results which become very stable in time. Computation of the projection at $t = 10T$ cannot give accurate results with the chosen value $R_0 = 10$ a.u., as we cut away too large of a part of the doubly ionized wave packet. For the results reported below, we used $t = 16T$.

2. Photon energy 75 eV

The TDCS of the DPI of H_2 at photon energy of 75 eV is shown in Fig. 3. The excess energy is shared equally between the photoelectrons. The top row displays the Π molecular orientation with the internuclear axis at the angle $\theta_N = 90^\circ$ to

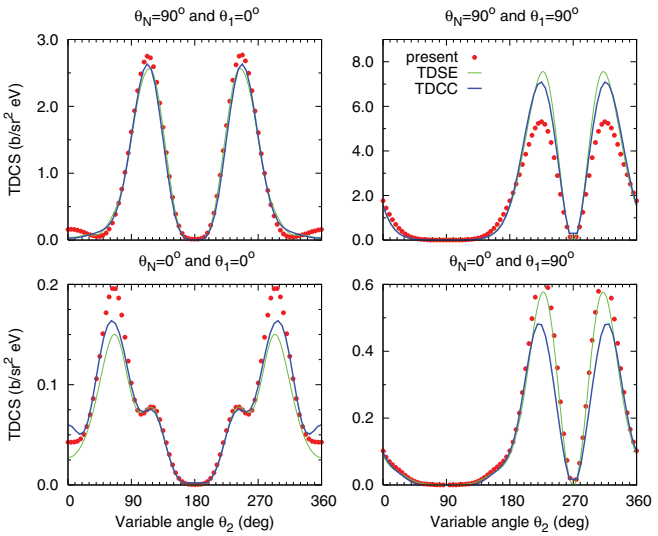

FIG. 3. (Color online) Coplanar TDCS of the DPI of H_2 at photon energy of 75 eV and equal energy sharing. The angle of the internuclear axis θ_N and the fixed reference photoelectron angle θ_1, both measured relative to the polarization vector of light, are indicated on each panel. The present spherical TDSE results are plotted with red filled circles, the prolate TDSE results [21] are shown with the thin green line, and the TDCC results [22] are exhibited by the thick blue line.

the linearly polarized xuv field. The bottom row displays the TDCS corresponding to the Σ orientation with $\theta_N = 0^\circ$. On the left and right columns, the reference photoelectron angle is fixed at $\theta_1 = 0^\circ$ and 90°, respectively. For each combination of angles θ_N and θ_1, a comparison is made with another two sets of time-dependent calculations: one is seeking the solution of the TDSE in prolate spheroidal coordinates [21], and another is employing the TDCC method [22].

In Fig. 3, a comparison is made on the absolute scale. Given the quite different shape, duration, and intensity of the field pulse assumed in these three models, agreement between the TDCS is rather satisfactory. The literature values [21,22] tend to converge better, except for the parallel-field orientation at $\theta_1 = 90^\circ$, where the present calculation and that of Ref. [21] agree between themselves but deviate somewhat from Ref. [22]. Generally, we may conclude that the present model is sufficiently accurate to capture the essential dynamics of the DPI process in H_2 and its orientation dependence.

In the atomiclike description of the DPI of H_2, which is restricted to the $S \to P$ transition in the electron-pair total angular momentum [8], the coplanar TDCS at the equal energy sharing can be represented by the following expression:

$$\frac{d^3\sigma}{dE d\theta_1 d\theta_2} = |(g_\Sigma \cos^2\theta_N + g_\Pi \sin^2\theta_N)(\cos\theta_1 + \cos\theta_2) + (g_\Sigma - g_\Pi)\cos\theta_N \sin\theta_N (\sin\theta_1 + \sin\theta_2)|^2. \quad (10)$$

Here the molecular-orientation angle θ_N and the photoelectron escape angles θ_1, θ_2 are counted from the direction of the polarization vector of light. The pair of amplitudes g_Σ and g_Π, which both depend on the mutual photoelectron angle $\theta_{12} = |\theta_1 - \theta_2|$, correspond to the parallel $\boldsymbol{e} \| \hat{\boldsymbol{R}}_N$ and

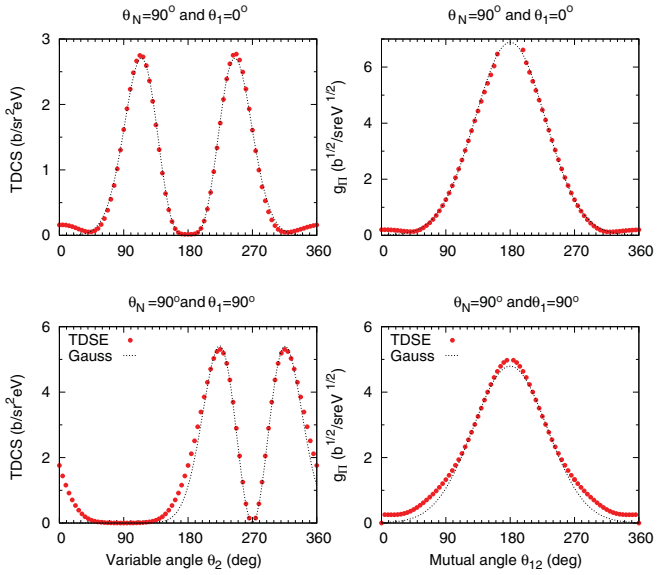

FIG. 4. (Color online) The presently calculated TDCS of Fig. 2 at $\theta_N = 90^\circ$ (left column) and the corresponding amplitude g_Π (right column) (both shown by the red dots) are fitted with the Gaussian ansatz (shown as a dotted line). The top and bottom rows correspond to the reference photoelectron angle fixed at $\theta_1 = 0^\circ$ and 90°, respectively.

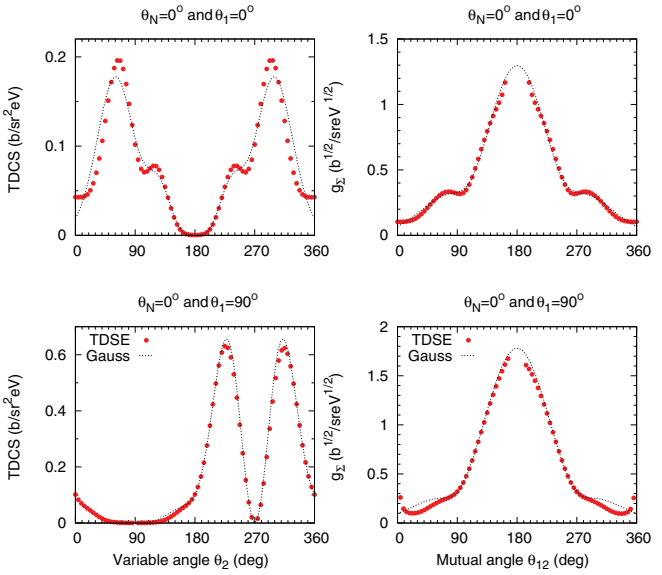

FIG. 5. (Color online) The TDCS of Fig. 2 at $\theta_N = 0^\circ$ (left column) and the corresponding amplitude g_Σ (right column) (both shown by the red dots) are fitted with the di-Gaussian ansatz (shown as a dotted line). The top and bottom rows correspond to the reference photoelectron angle fixed at $\theta_1 = 0^\circ$ and 90°, respectively.

perpendicular $\boldsymbol{e} \perp \hat{\boldsymbol{R}}_N$ molecular orientations, respectively. The TDCS formula (10) can be inverted to yield the moduli of the amplitudes,

$$|g_{\Sigma\,\text{or}\,\Pi}(\theta_{12})| = \left[\frac{d^3\sigma(\theta_N = 0^\circ \text{ or } 90^\circ)}{dE d\theta_1 d\theta_2}\right]^{1/2} \frac{1}{\cos\theta_1 + \cos\theta_2}. \tag{11}$$

In Figs. 4 and 5, we use this expression to obtain the amplitudes g_Σ and g_Π from the presently calculated TDCS exhibited in Fig. 3. Thus, we obtain the amplitudes for all values of θ_{12}, except for a small interval around $\theta_{12} = 180^\circ$ where the kinematic factor $\cos\theta_1 + \cos\theta_2$ tends to zero.

When inspecting Fig. 4, we observe that the modulus of the amplitude g_Π can be fitted very well with the Gaussian ansatz,

$$|g_\Pi(\theta_{12})| = A \exp\left[-2\ln 2 \frac{(180^\circ - \theta_{12})^2}{\Delta\theta^2}\right]. \tag{12}$$

The Gaussian magnitude A and width $\Delta\theta$ parameters derived from the TDCS for perpendicular-field orientation $\theta_N = 90^\circ$ and the reference photoelectron angles $\theta_1 = 0^\circ$ and 90° are shown in Table I. In the same table, we present the analogous values derived from the TDCS produced by other methods [21,22]. The difference between the pair of the Gaussian parameters derived from TDCS at $\theta_1 = 0^\circ$ and 90° serves as an indication of the accuracy of the atomiclike expression (10). For an atomic target, these parameters should be identical. Surprisingly, these parameters are very close for the perpendicular orientation of the H_2 molecule as well, especially in the prolate TDSE calculation [22].

A similar extraction of the g_Σ amplitude from the TDCS at the parallel field $\theta_N = 0^\circ$ is illustrated in Fig. 5. In this case, in stark contrast to the perpendicular orientation at $\theta_N = 90^\circ$, the amplitude g_Σ is manifestly non-Gaussian. A similar shape of the amplitude was encountered when analyzing the TDCS of the DPI of various atomic targets containing an L shell [27]. It can be represented by a superposition of two Gaussians, each containing its own set of magnitude and width parameters:

$$|g_\Sigma(\theta_{12})| = \left| A_1 \exp\left[-2\ln 2\left(\frac{180^\circ - \theta_{12}}{\Delta\theta_1}\right)^2\right] + e^{i\phi} A_2 \exp\left[-2\ln 2\left(\frac{180^\circ - \theta_{12}}{\Delta\theta_2}\right)^2\right]\right|. \tag{13}$$

The phase shift ϕ in Eq. (13) is usually close to π.

The amplitude g_Σ has two prominent features. Similarly to the amplitude g_Π, it shows a Gaussian-like peak at the back-to-back emission corresponding to $\theta_{12} = 180^\circ$. In addition, it has a shoulder at about 70°. In the atomiclike description of the DPI process (10), the back-to-back emission with equal energy sharing is strongly forbidden by the dipole selection rule [34]. So the kinematic factor $\cos\theta_1 + \cos\theta_2$ and the dynamic amplitude factor should "negotiate" a compromise angle where

TABLE I. Gaussian magnitude A and width $\Delta\theta$ parameters of the symmetric amplitude g_Π derived from the TDCS for perpendicular-field orientation $\theta_N = 90^\circ$ and the reference photoelectron angles $\theta_1 = 0^\circ$ and 90°.

	Magnitude A_Π ($b^{1/2}$/sr eV$^{1/2}$)		Width $\Delta\theta_\Pi$ (deg)	
	$\theta_1 = 0^\circ$	$\theta_1 = 90^\circ$	$\theta_1 = 0^\circ$	$\theta_1 = 90^\circ$
Present	6.8	4.8	82	86
TDSE [21]	6.7	6.0	81	82
TDCC [22]	6.5	5.5	82	86

TABLE II. Di-Gaussian magnitude A_1, A_2, width $\Delta\theta_1$, $\Delta\theta_2$, and phase shift ϕ parameters of the symmetric amplitude g_Σ derived from the TDCS for parallel-field orientation $\theta_N = 0^\circ$ and the reference photoelectron angle $\theta_1 = 0^\circ$.

	Magnitude ($b^{1/2}$/sr $eV^{1/2}$)		Width (deg)		Phase (rad)
	A_1	A_2	$\Delta\theta_1$	$\Delta\theta_2$	ϕ
Present	7.6	6.6	96	107	−3.02
TDSE [21]	4.9	3.9	93	108	−2.95
TDCC [22]	4.9	4.2	102	116	−2.97

the TDCS reaches its maximum. With a simple Gaussian shape of the amplitude g_Σ, this maximum is reached at a mutual electron angle $\theta_{12} \simeq 120^\circ$, i.e., the photoelectrons escape predominantly in the opposite directions. With a non-Gaussian amplitude g_Σ, this situation changes dramatically. Indeed, at the fixed reference electron angle $\theta_1 = 0^\circ$, the TDCS reaches its maximum exactly where the amplitude g_Σ has its shoulder, i.e., $\theta_{12} \simeq 70^\circ$. This corresponds to the photoelectron escaping predominantly to the same direction. This behavior is exhibited clearly in Fig. 8 of Ref. [21], albeit without a qualitative physical explanation. At another fixed reference electron angle of $\theta_1 = 90^\circ$, the maximum of the TDCS is moved away from the shoulder of g_Σ, which is not so prominent as in the case of $\theta_1 = 0^\circ$.

The di-Gaussian parameters of the amplitude g_Σ, derived from the TDCS at the angles $\theta_N = \theta_1 = 0^\circ$, are given in Table II for the present calculation in comparison with the other two sets of data [21,22]. The width parameters of g_Σ are larger than that of g_Π. In the atomic DPI, the width parameter is determined by the size of the ionic core left behind by the primary photoelectron. A tighter core corresponds to a larger Gaussian width, and, conversely, a sparse core, extended in coordinate space, defines a narrow Gaussian [27,35]. An explanation of this empirical rule can be traced to the two-step mechanism of the atomic DPI, which is dominant at the photon energies not far away from the threshold. In this mechanism, the DPI proceeds via single photoionization and subsequent electron-impact ionization of the singly charged positive ion. On this second stage, a smaller number of partial waves can reach a compact ionic orbital because of the centrifugal barrier. As the angular width and the angular momentum are the conjugate variables, fewer partial waves comprise a wider Gaussian.

The deviation from a simple Gaussian shape of the symmetric amplitude in the atomic DPI can be related to an extra node of the L-shell target orbital [27]. Similar arguments can be applied to the present case of the DPI of the aligned H_2 molecule. As is shown in Figs. 4 and 5 of Ref. [26], at photon energy of 75 eV, the photoelectrons are aligned strongly with the field polarization vector. This means that they impinge on the molecular H_2^+ ion parallel and perpendicular to the internuclear axis in the Σ and Π orientations, respectively. The properties of the H_2^+ wave function in these two directions are manifestly different [36]. Going from the center of the molecular ion in the perpendicular direction, the projectile encounters a smooth wave function which has neither nodes

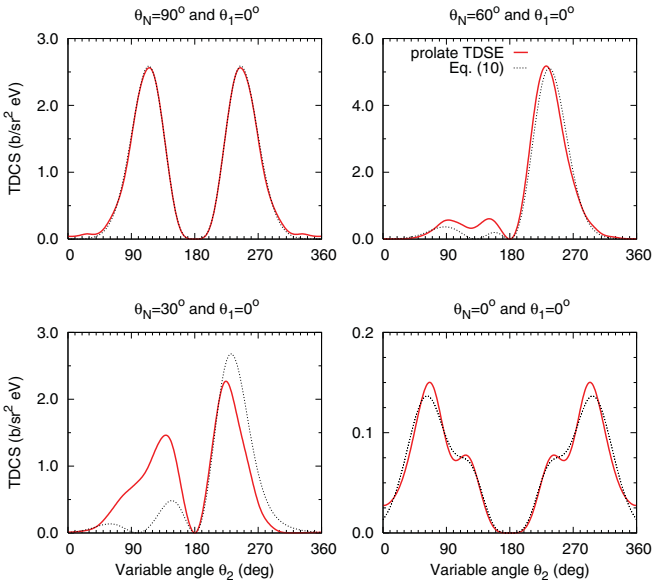

FIG. 6. (Color online) Equal energy sharing coplanar TDCS of the DPI of H_2 at various angles of the internuclear axis, $\theta_N = 90^\circ$, 60°, 30°, and 0°, relative to the polarization vector of light. The reference photoelectron angle is fixed at $\theta_1 = 0^\circ$. The red solid line represent the prolate TDSE calculation of Ref. [21]. The dotted line represents Eq. (10), with the amplitudes g_Π and g_Σ parametrized using the corresponding entries in Tables I and II.

nor singularities. In the parallel direction, the same route crosses a strong Coulomb singularity on the nucleus.

Until now, we applied Eq. (10) to the two "pure" cases of parallel and perpendicular molecular orientation when only one of the amplitudes g_Π and g_Σ defines the TDCS. To test this atomiclike expression for mixed cases, we use the complete set of the TDCS reported in Ref. [21]. We generate the amplitudes g_Π and g_Σ from the corresponding parameters tabulated in Tables I and II. Then we feed these amplitudes into Eq. (10) for various field orientations corresponding to $\theta_N = 90^\circ$, 60°, 30°, and 0°, and the reference photoelectron angle $\theta_1 = 0$. We compare thus generated results with *ab initio* calculations presented in Fig. 5 of Ref. [21]. This comparison is illustrated in Fig. 6. In principle, the amplitudes g_Π and g_Σ should be treated as complex variables. However, the phase information cannot be retrieved from the TDCS analysis. So we ignore the phase difference between g_Π and g_Σ. Nevertheless, the obtained "synthetic" TDCS match their *ab initio* counterparts rather well. This indicates that the atomiclike description of the coplanar TDCS is generally valid for H_2.

Finally, in Fig. 7, we present the TDCS for the perpendicular geometry when one of the two photoelectrons is detected out of the plane made by the internuclear axis $\hat{\boldsymbol{R}}_N$ and the polarization vector $\boldsymbol{e}$. Generally, agreement with the two other time-dependent calculations [21,22] is satisfactory.

For this perpendicular geometry, the atomiclike formula (10) reads

$$\frac{d^3\sigma_{\Pi\text{ or }\Sigma}}{dE\,d\theta_1\,d\theta_2} = |g_{\Sigma\text{ or }\Pi}(\theta_{12} = 90^\circ)|^2 \cos^2\theta_2, \qquad (14)$$

where the amplitudes g_Π or g_Σ are chosen for the angles $\theta_N = 90^\circ$ and $\theta_N = 0^\circ$, respectively. The pure $\cos^2\theta_2$ dependence is

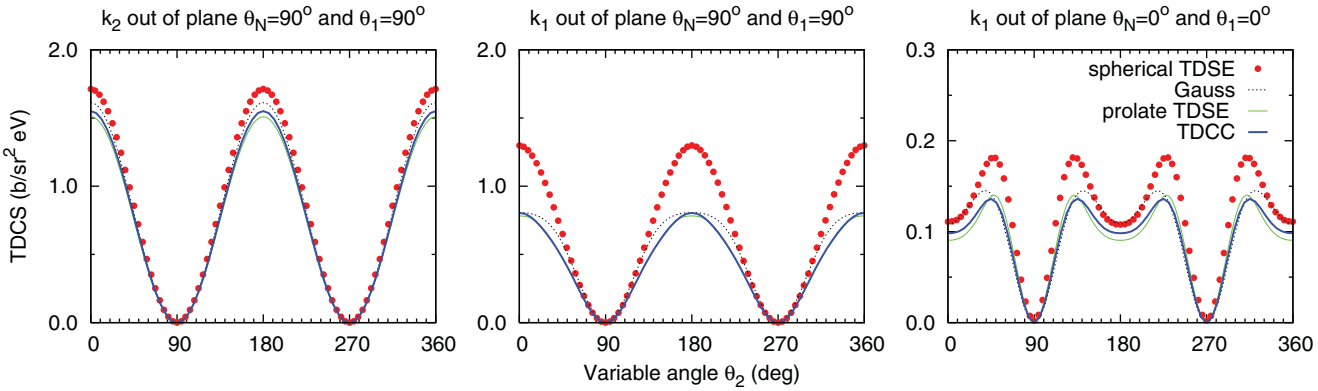

FIG. 7. (Color online) Noncoplanar TDCS of the aligned hydrogen molecule for equal energy sharing. The present spherical TDSE results (red solid dots) are compared with the prolate TDSE (green thin line) [21] and TDCC [22] predictions (blue thick line). The dotted line indicates the results obtained by using the amplitudes g_Π (left and middle panels) and g_Σ (right panel) with the Gaussian parameters tabulated in Tables I and II, respectively.

clearly observed on the left panel of Fig. 7, but it is decisively broken on the right panel. Feagin *et al.* [28] suggested that the atomiclike description (10) can still be applied in the case of perpendicular geometry. However, the dipole kinematic factor $(\cos\theta_1 + \cos\theta_2)^2$, which is the signature of the $S \to P$ transition in the total angular momentum of the photoelectron pair, should be replaced by a more general expression to account for $S \to D$ and $S \to F$ transitions. On the left panel of Fig. 7, we use the amplitude g_Π generated from the Gaussian parameters of Table I to represent the TDCS according to Eq. (14). Agreement with *ab initio* results is indeed very good in this case. On the central and right panels of Fig. 7, we repeat this procedure. However, we modify the kinematic factor $\cos^2\theta_2$ by additional multipliers $0.5(1 + 0.4\sin^2\theta_2)^2$ (middle panel) and $(1 + 0.23\sin^2\theta_2)^2$ (right panel), as prescribed in Ref. [28]. This procedure gives us very satisfactory results, thus demonstrating the utility of the amplitude analysis in a rather general case.

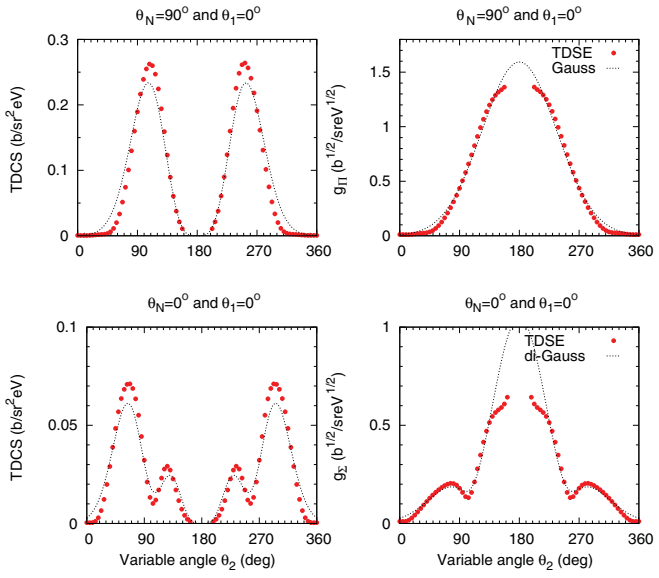

FIG. 8. (Color online) Left: Coplanar TDCS of the DPI of H_2 at photon energy of 120 eV and equal energy sharing. The angle of the internuclear axis $\theta_N = 90^\circ$ (top) and 0° (bottom) and the fixed reference photoelectron angle $\theta_1 = 0$. Right: corresponding amplitude g_Π (top) and g_Σ (bottom) (both shown by the red dots) are fitted with the Gaussian ansatz (12) and di-Gaussian ansatz (13), respectively.

3. *Photon energy 120 eV*

This photon energy is chosen to be well outside the Cooper-like minimum in the dipole channel of single photoionization of H_2 for the Σ orientation. By analyzing the TDCS at this photon energy and extracting the amplitudes via Eq. (10), we can check if the strongly non-Gaussian shape of the amplitude g_Σ is somehow related to this minimum. This analysis is presented in Fig. 8. From this figure, we can see that very similarly to the previous case of the photon energy of 75 eV, the amplitude g_Π is Gaussian whereas the amplitude g_Σ is not. This observation makes us believe that it is a general wave-function structure of the H_2^+ ion that is responsible for this behavior, rather than the Cooper-like minimum in the dipole Π channel at a specific photon energy of 75 eV.

IV. CONCLUSIONS

In the present work, we solve the time-dependent Schrödinger equation for the H_2 molecule exposed to an xuv pulse. By propagating this solution in time outside the pulse interval and projecting it on the field-free continuum states of the H_2^+ molecular ion, we derive the fully integrated as well as triply differential cross sections (TDCS) of the double photoionization of $H_2$with a given orientation of the internuclear axis relative to the polarization vector of light. We test these found cross sections against the most recent and consistent literature values and find generally good agreement. This validates our numerical model.

We use the coplanar TDCS at the parallel- and perpendicular-molecular-field mutual orientation to derive the symmetric amplitudes g_Π and g_Σ, which contain the most essential dynamical information of the DPI process at the

equal energy sharing. These amplitudes are fitted with a simple Gaussian and di-Gaussian ansatz, respectively. This shape of the amplitudes explains the peculiarities of the coplanar TDCS, in particular, the prevalence of the same direction of escape of the photoelectrons at the parallel-molecular-field orientation.

The amplitude information obtained from the TDCS is incomplete, as the mutual phase of the amplitudes g_Π and g_Σ is missing. It would be more instructive to derive these amplitudes fully *ab initio*, as can be done in the atomic case (see, e.g., Ref. [37]). With complete amplitude information, the tests of the orientation dependence of the coplanar TDCS can be made more convincing. Also, it would be interesting to perform this amplitude analysis at various internuclear distances. By increasing this distance from equilibrium, we can make the Π or Σ anisotropy stronger.

Finally, it would be very instructive to perform explicit calculations of the electron-impact ionization of the H_2^+ molecular ion and to compare the angular correlation pattern in the $(\gamma,2e)$ reaction on $H_2$and the $(e,2e)$ reaction on H_2^+ at the corresponding incident energies. In the atomic case, these patterns are found to be very similar [27].

ACKNOWLEDGMENTS

We are grateful to James Colgan, Xiaoxu Guan, and Klaus Bartschat for communicating their data in numerical form. The authors acknowledge the support of the Australian Research Council in the form of Discovery Grant No. DP0985136. The facilities of the National Computational Infrastructure (NCI) National Facility were used.

[1] T. Weber *et al.*, Nature (London) **431**, 437 (2004).
[2] T. Weber *et al.*, Phys. Rev. Lett. **92**, 163001 (2004).
[3] M. Gisselbrecht, M. Lavollée, A. Huetz, P. Bolognesi, L. Avaldi, D. P. Seccombe, and T. J. Reddish, Phys. Rev. Lett. **96**, 153002 (2006).
[4] T. J. Reddish, J. P. Wightman, M. A. MacDonald, and S. Cvejanović, Phys. Rev. Lett. **79**, 2438 (1997).
[5] J. P. Wightman, S. Cvejanovic, and T. J. Reddish, J. Phys. B **31**, 1753 (1998).
[6] N. Scherer, H. Lörch, and V. Schmidt, J. Phys. B **31**, L817 (1998).
[7] D. P. Seccombe, S. A. Collins, T. J. Reddish, P. Selles, L. Malegat, A. K. Kazansky, and A. Huetz, J. Phys. B **35**, 3767 (2002).
[8] J. M. Feagin, J. Phys. B **31**, L729 (1998).
[9] T. J. Reddish and J. M. Feagin, J. Phys. B **32**, 2473 (1999).
[10] A. S. Kheifets, Phys. Rev. A **71**, 022704 (2005).
[11] A. S. Kheifets and I. Bray, Phys. Rev. A **72**, 022703 (2005).
[12] J. Colgan, M. S. Pindzola, and F. Robicheaux, J. Phys. B **37**, L377 (2004).
[13] W. Vanroose, F. Martín, T. N. Rescigno, and C. W. McCurdy, Phys. Rev. A **70**, 050703 (2004).
[14] G. Dujardin, M. J. Besnard, L. Hellner, and Y. Malinovitch, Phys. Rev. A **35**, 5012 (1987).
[15] H. Kossmann, O. Schwarzkopf, B. Kämmerling, and V. Schmidt, Phys. Rev. Lett. **63**, 2040 (1989).
[16] H. L. Rouzo, J. Phys. B **19**, L677 (1986).
[17] H. Le Rouzo, Phys. Rev. A **37**, 1512 (1988).
[18] W. Vanroose, F. Martín, T. N. Rescigno, and C. W. McCurdy, Science **310**, 1787 (2005).
[19] J. Colgan, M. S. Pindzola, and F. Robicheaux, Phys. Rev. Lett. **98**, 153001 (2007).
[20] L. Tao, C. W. McCurdy, and T. N. Rescigno, Phys. Rev. A **82**, 023423 (2010).
[21] X. Guan, K. Bartschat, and B. I. Schneider, Phys. Rev. A **83**, 043403 (2011).
[22] J. Colgan (private communication).
[23] M. G. Pullen *et al.*, Opt. Lett. **36**, 3660 (2011).
[24] I. A. Ivanov and A. S. Kheifets, Phys. Rev. A **75**, 033411 (2007).
[25] M. Schuricke, G. Zhu, J. Steinmann, K. Simeonidis, I. Ivanov, A. Kheifets, A. N. Grum-Grzhimailo, K. Bartschat, A. Dorn, and J. Ullrich, Phys. Rev. A **83**, 023413 (2011).
[26] S. K. Semenov and N. A. Cherepkov, J. Phys. B **36**, 1409 (2003).
[27] A. S. Kheifets, I. Bray, J. Colgan, and M. S. Pindzola, J. Phys. B **44**, 011002 (2011).
[28] J. M. Feagin, J. Colgan, A. Huetz, and T. J. Reddish, Phys. Rev. Lett. **103**, 033002 (2009).
[29] D. A. Varshalovich, A. N. Moskalev, and V. K. Khersonskii, *Quantum Theory of Angular Momentum* (World Scientific, Singapore, 1988).
[30] T. J. Park and J. C. Light, J. Chem. Phys. **85**, 5870 (1986).
[31] D. Dundas, Phys. Rev. A **65**, 023408 (2002).
[32] L. B. Madsen, L. A. A. Nikolopoulos, T. K. Kjeldsen, and J. Fernández, Phys. Rev. A **76**, 063407 (2007).
[33] J. Colgan and M. S. Pindzola, Phys. Rev. Lett. **88**, 173002 (2002).
[34] F. Maulbetsch and J. S. Briggs, J. Phys. B **28**, 551 (1995).
[35] A. S. Kheifets and I. Bray, Phys. Rev. A **73**, 020708 (2006).
[36] D. R. Bates, K. Ledsham, and A. L. Stewart, Philos. Trans. R. Soc. London A **246**, 215 (1953).
[37] A. S. Kheifets and I. Bray, Phys. Rev. A **62**, 065402 (2000).